Two Cylindrical Obstacles in a Rectangular Waveguide—Resonances and Filter Applications

ROLAND GESCHE, MEMBER, IEEE, AND NORBERT LÖCHEL

Abstract—Two metallic or lossy dielectric cylinders placed in one cross section of a rectangular waveguide are investigated by means of the orthogonal expansion method. Resonances are shown by frequency responses of the transmission coefficient. They are discussed by patterns of the magnetic field and diagrams of the Poynting vector. Physical explanations of the resonances are given.

The structure may be used as a filter element. With two small dielectric posts, a frequency characteristic with two stopbands can be obtained. Center frequencies are tunable by moving the posts. Using one large metallic and one small dielectric post, a tunable passband characteristic can be realized.

I. Introduction

CYLINDRICAL dielectric or metallic posts in a rectangular waveguide can be used to realize several filter characteristics. A single lossy dielectric cylinder in a rectangular waveguide has been discussed in [1]. In the present work, the method used in [1] has been extended to two posts positioned in one cross section of a rectangular waveguide [2]. The structure is shown in Fig. 1 and the following restrictions are considered:

- Incident fields are of the TE_{m0} mode.
- The axes of the cylindrical obstacles are parallel to the electric field vector.
- The post materials are assumed to be isotropic, homogeneous, and linear; they may have losses.
- The obstacles extend over the entire waveguide height.
- The waveguide walls are ideal conductors.

An overview of previous papers which investigate the one-post structure is given in [1]. Filter applications have been discussed by Lauterjung [3] and Sahalos and Vafiadis [4]. Methods to calculate multiple-post structures are given in [5]–[7]. A lumped-element representation of a lossy post has been discussed in [8].

Manuscript received September 14, 1988; revised December 29, 1988.

R. Gesche is with Leybold AG, Siemensstrasse 100, 8755 Alzenau, West Germany.

N. Löchel is with the Transmission Systems Division, Siemens AG, 8000 München, West Germany.

IEEE Log Number 8927166.

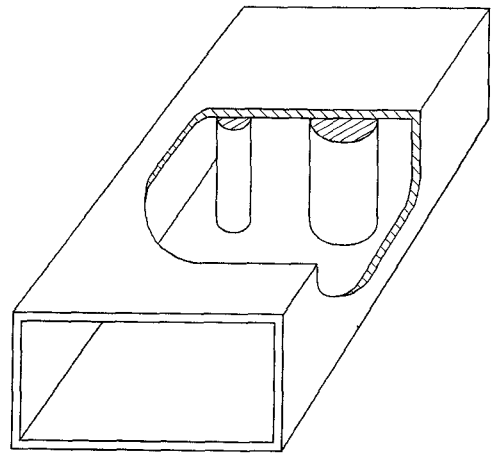

Fig. 1. Rectangular waveguide with two cylindrical posts.

II. Mathematical Formulation

The mathematical formulation is based on the calculation of a single dielectric post given in [1]. In the following, only the fundamental equations and the modifications of [1] are given.

The geometry of the structure and the coordinate systems are shown in Fig. 2. Each post is located at the origin of a cylindrical coordinate system (ρ_1^S, φ_1^S, z and ρ_2^S, φ_2^S, z, respectively). Furthermore, two cylindrical interaction regions (IR1 and IR2) are introduced with the coordinate systems ρ_1, φ_1, z and ρ_2, φ_2, z, respectively. Each interaction region includes one obstacle; together they cover the entire cross section of the rectangular waveguide. This cross section divides the rectangular waveguide into two regions, named W1 and W2.

The fields of the incident TE_{m0} mode and all scattered fields are independent of the z coordinate. Therefore, it is sufficient to consider only three field components: one electrical field component parallel to the post axes and two perpendicular magnetic field components. These fields can be derived from a vector potential:

$$\vec{A} = A_z \vec{e}_z e^{j\omega t} \qquad \vec{H} = \nabla \times \vec{A} \qquad \vec{E} = \frac{1}{j\omega\epsilon}(\nabla \times \vec{H}). \tag{1}$$

0018-9480/89/0600-0962$01.00 ©1989 IEEE

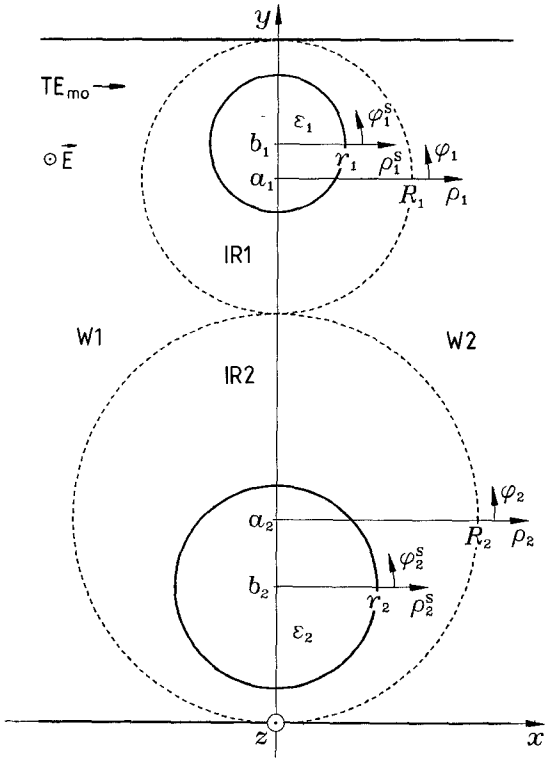

Fig. 2. Geometry of the investigated structure.

Perfectly conducting metallic and lossy dielectric materials are considered by the permittivity:

$$\epsilon = \begin{cases} \epsilon_1 = \begin{cases} \epsilon_0\epsilon_{r1}(1 - j\tan\delta_1) \\ \text{or} \\ -j\infty \end{cases} & \text{inside post 1} \\ \epsilon_2 = \begin{cases} \epsilon_0\epsilon_{r2}(1 - j\tan\delta_2) \\ \text{or} \\ -j\infty \end{cases} & \text{inside post 2} \\ \epsilon_0 & \text{outside the posts.} \end{cases} \tag{2}$$

A. Fields in the Interaction Regions

In both interaction regions, a field formulation in the regions outside the posts ($\rho_i \geq r_i + |b_i - a_i|$) is chosen using the radial functions $U_{i0}(k\rho_i)$, $U_{ip}^s(k\rho_i)$, $U_{ip}^c(k\rho_i)$ defined in [1]:

$$A_z = U_{i0}(k\rho_i)\frac{1}{\sqrt{2\pi}} + \sum_{p=1}^{\infty}\left\{U_{ip}^s(k\rho_i)\frac{\sin p\varphi_i}{\sqrt{\pi}} + U_{ip}^c(k\rho_i)\frac{\cos p\varphi_i}{\sqrt{\pi}}\right\}, \quad i = 1,2. \tag{3}$$

The subscript i marks the interaction regions IR1 and IR2, respectively.

The separation condition yields

$$k = \omega\sqrt{\epsilon_0\mu_0}. \tag{4}$$

A_z is proportional to the electric field component E_z. A further function, which is proportional to the magnetic field components H_{φ_i}, is defined as

$$H_{\varphi_i}h = -\frac{\partial A_z}{\partial\rho}h = I_{i0}(k\rho_i)\frac{1}{\sqrt{2\pi}} + \sum_{p=1}^{\infty}\left\{I_{ip}^s(k\rho_i)\frac{\sin p\varphi_i}{\sqrt{\pi}} + I_{ip}^c(k\rho_i)\frac{\cos p\varphi_i}{\sqrt{\pi}}\right\}, \quad i = 1,2 \tag{5}$$

where h is the waveguide width $2(a_1 + a_2)$, which is used as the normalization length.

Each scattering obstacle is introduced by a matrix equation for the amplitude vectors of the field formulations (3) and (5) as described in [1]:

$$\vec{U}_i(k\rho_i) = \underline{Z}_i(k\rho_i)\cdot\vec{I}_i(k\rho_i) \qquad i = 1,2. \tag{6}$$

B. Scattering Parameters

In the rectangular waveguide regions W1 and W2, fields of the TE_{m0} modes are considered:

Waveguide region W1:

$$A_z = \sum_{m=1}^{\infty}\sin\frac{m\pi y}{h}\left\{q_m e^{-jk_{xm}x} + r_m e^{+jk_{xm}x}\right\}. \tag{7}$$

Waveguide region W2:

$$A_z = \sum_{m=1}^{\infty}\sin\frac{m\pi y}{h}\left\{t_m e^{-jk_{xm}x} + s_m e^{+jk_{xm}x}\right\} \tag{8}$$

$$k_{xm} = \sqrt{\omega^2\epsilon_0\mu_0 - \left[\frac{m\pi}{h}\right]^2}. \tag{9}$$

An expansion of the fields (7) and (8) in terms of the φ_i-dependent orthogonal eigenfunctions of the fields (3) and (5) on the surfaces of the interaction regions yields relations between the amplitude vectors (the explicit formulas for the coupling matrices $\underline{K}^{UE}$, $\underline{K}^{UA}$, $\underline{K}^{IE}$, and $\underline{K}^{IA}$ are given in [1]):

$$\vec{U}_i(kR_i) = \underline{K}_i^{UE}\cdot\begin{bmatrix} q_1 \\ q_2 \\ \vdots \\ s_1 \\ s_2 \\ \vdots \end{bmatrix} + \underline{K}_i^{UA}\cdot\begin{bmatrix} r_1 \\ r_2 \\ \vdots \\ t_1 \\ t_2 \\ \vdots \end{bmatrix} \qquad i = 1,2 \tag{10}$$

$$\vec{I}_i(kR_i) = \underline{K}_i^{IE}\cdot\begin{bmatrix} q_1 \\ q_2 \\ \vdots \\ s_1 \\ s_2 \\ \vdots \end{bmatrix} + \underline{K}_i^{IA}\cdot\begin{bmatrix} r_1 \\ r_2 \\ \vdots \\ t_1 \\ t_2 \\ \vdots \end{bmatrix} \qquad i = 1,2. \tag{11}$$

Equations (10) and (11) are combined, forming a new

interaction region from IR1 and IR2 which extends over the entire cross section of the rectangular waveguide and which is described by the amplitude vectors of IR1 and IR2:

$$\begin{bmatrix} \vec{U}_1(kR_1) \\ \vec{U}_2(kR_2) \end{bmatrix} = \begin{bmatrix} \underline{K}_1^{UE} \\ \underline{K}_2^{UE} \end{bmatrix} \cdot \begin{bmatrix} q_1 \\ q_2 \\ \vdots \\ s_1 \\ s_2 \\ \vdots \end{bmatrix} + \begin{bmatrix} \underline{K}_1^{UA} \\ \underline{K}_2^{UA} \end{bmatrix} \cdot \begin{bmatrix} r_1 \\ r_2 \\ \vdots \\ t_1 \\ t_2 \\ \vdots \end{bmatrix} \quad (12)$$

$$\begin{bmatrix} \vec{I}_1(kR_1) \\ \vec{I}_2(kR_2) \end{bmatrix} = \begin{bmatrix} \underline{K}_1^{IE} \\ \underline{K}_2^{IE} \end{bmatrix} \cdot \begin{bmatrix} q_1 \\ q_2 \\ \vdots \\ s_1 \\ s_2 \\ \vdots \end{bmatrix} + \begin{bmatrix} \underline{K}_1^{IA} \\ \underline{K}_2^{IA} \end{bmatrix} \cdot \begin{bmatrix} r_1 \\ r_2 \\ \vdots \\ t_1 \\ t_2 \\ \vdots \end{bmatrix}. \quad (13)$$

The scattering matrix can be derived from (12) and (13) using (6):

$$\begin{bmatrix} r_1 \\ r_2 \\ \vdots \\ t_1 \\ t_2 \\ \vdots \end{bmatrix} = \underline{S} \cdot \begin{bmatrix} q_1 \\ q_2 \\ \vdots \\ s_1 \\ s_2 \\ \vdots \end{bmatrix} \quad (14)$$

$$\underline{S} = \left\{ \begin{bmatrix} \underline{K}_1^{UA} \\ \underline{K}_2^{UA} \end{bmatrix} - \begin{bmatrix} \underline{Z}_1(kR_1) & 0 \\ 0 & \underline{Z}_2(kR_2) \end{bmatrix} \cdot \begin{bmatrix} \underline{K}_1^{IA} \\ \underline{K}_2^{IA} \end{bmatrix} \right\}^{-1} \cdot \left\{ \begin{bmatrix} \underline{Z}_1(kR_1) & 0 \\ 0 & \underline{Z}_2(kR_2) \end{bmatrix} \cdot \begin{bmatrix} \underline{K}_1^{IE} \\ \underline{K}_2^{IE} \end{bmatrix} - \begin{bmatrix} \underline{K}_1^{UE} \\ \underline{K}_2^{UE} \end{bmatrix} \right\}. \quad (15)$$

C. Numerical Investigation

The mathematical formulation described above is exact. For numerical investigation, all infinite sums must be approximated by finite sums. Convergence of scattering parameters and fields yield criteria for the accuracy of the results. Conditions for the relations of the wavenumbers in the different regions are given by the mathematical method used. The sum of waves in both interaction regions ($2p_{\max 1} + 2p_{\max 2} + 2$) must be equal to the sum of waves in the rectangular waveguide regions ($m_{\max 1} + m_{\max 2}$). It is suitable to consider the same wavenumbers in both rectangular waveguide regions ($m_{\max 1} = m_{\max 2} = m_{\max}$). This yields the condition

$$m_{\max} = p_{\max 1} + p_{\max 2} + 1. \quad (16)$$

If the sizes of the interaction regions are nearly equal ($R_1 \approx R_2$), the wavenumbers should also be equal ($p_{\max 1} = p_{\max 2}$). Patterns of the magnetic fields for different wavenumbers are shown in Fig. 3. The convergence is obvious; for $p_{\max 1} = p_{\max 2} = 14$ the errors of the field matching become negligible. In this case, the accuracy of the scattering parameters of the fundamental mode is better than 1 percent. A further increase in wavenumbers yields no improvement in the results because of increasing numerical errors (a double-precision arithmetic was used). For higher wavenumbers, a more precise numerical treatment is necessary. So the example given represents the numerical limit of the mathematical method related to the computer system (Fortran 77, IBM 4381). The following results are given for smaller post sizes, so an accuracy better than 1 percent can be obtained with following wavenumbers:

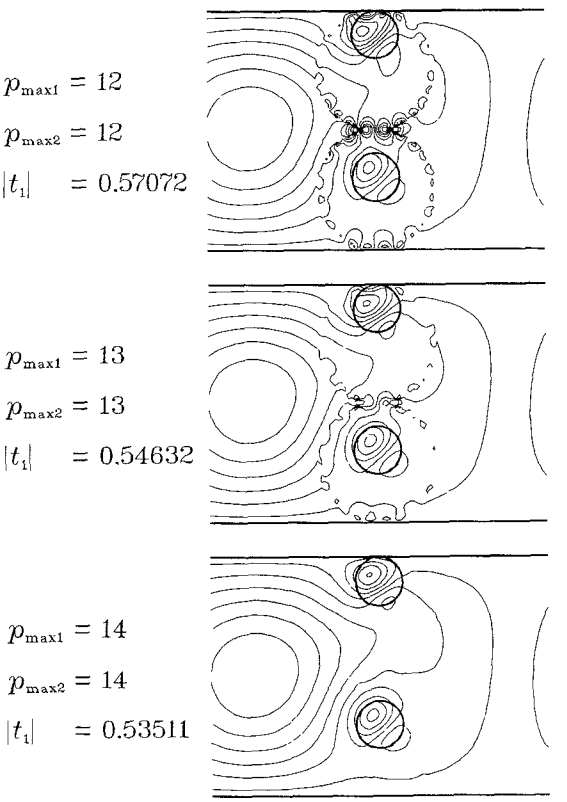

Fig. 3. Convergence of magnetic fields:

$f_n = 1.4$	$\omega t = 0.5\pi$
$\epsilon_{r1} = 38.5$	$\epsilon_{r2} = 38.5$
$\tan\delta_1 = 2\times10^{-4}$	$\tan\delta_2 = 2\times10^{-4}$
$r_1 = 0.1h$	$r_2 = 0.1h$
$b_1 = 0.9h$	$b_2 = 0\,3h.$

$$p_{\max 1} = p_{\max 2} = 14 \qquad m_{\max} = 29. \quad (17)$$

III. Results

Results are given for some examples of filter elements. With two dielectric posts, two bandstop resonances occur. Furthermore, a tunable passband characteristic can be obtained with one large metallic and one small dielectric post.

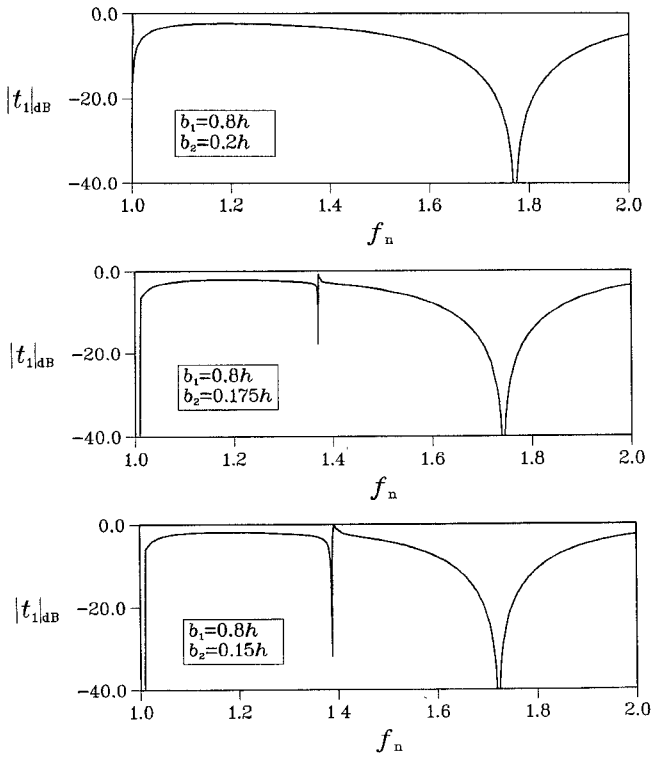

Fig. 4. Frequency responses showing the occurrence of a second stopband of a filter with two dielectric posts:

$\epsilon_{r1} = 38.5$ $\epsilon_{r2} = 38.5$
$\tan\delta_1 = 2\times10^{-4}$ $\tan\delta_2 = 2\times10^{-4}$
$r_1 = 0.03h$ $r_2 = 0.03h$.

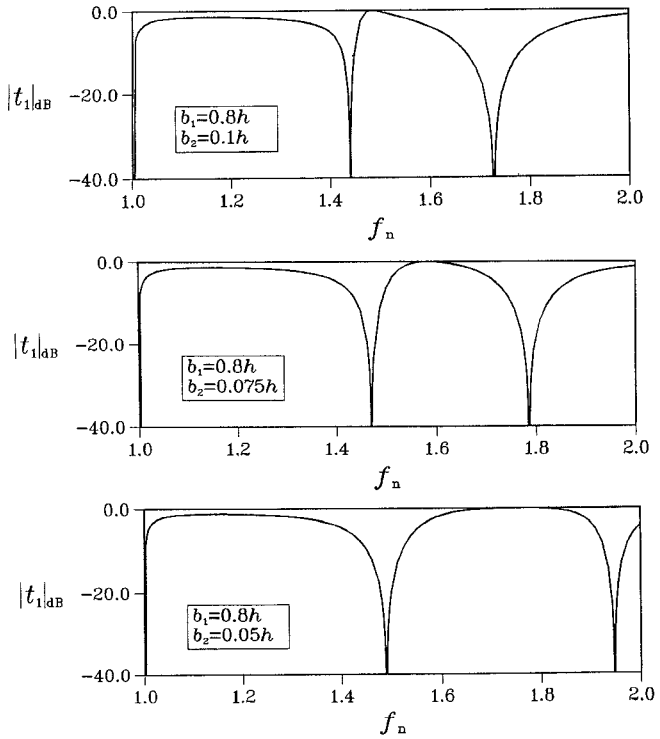

Fig. 5. Frequency responses showing the tuning of the upper stopband by moving the lower dielectric post:

$\epsilon_{r1} = 38.5$ $\epsilon_{r2} = 38.5$
$\tan\delta_1 = 2\times10^{-4}$ $\tan\delta_2 = 2\times10^{-4}$
$r_1 = 0.03h$ $r_2 = 0.03h$.

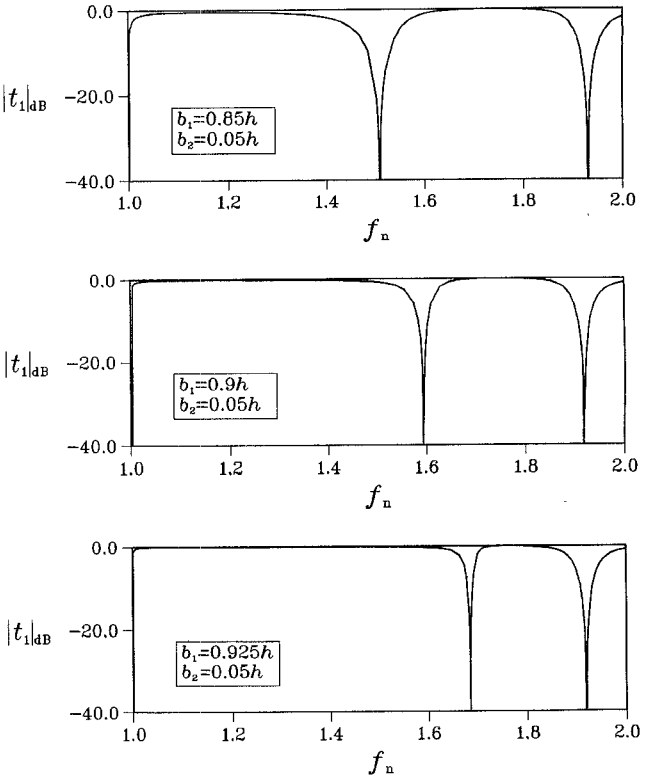

Fig. 6. Frequency responses showing the tuning of the lower stopband by moving the upper dielectric post:

$\epsilon_{r1} = 38.5$ $\epsilon_{r2} = 38.5$
$\tan\delta_1 = 2\times10^{-4}$ $\tan\delta_2 = 2\times10^{-4}$
$r_1 = 0.03h$ $r_2 = 0.03h$.

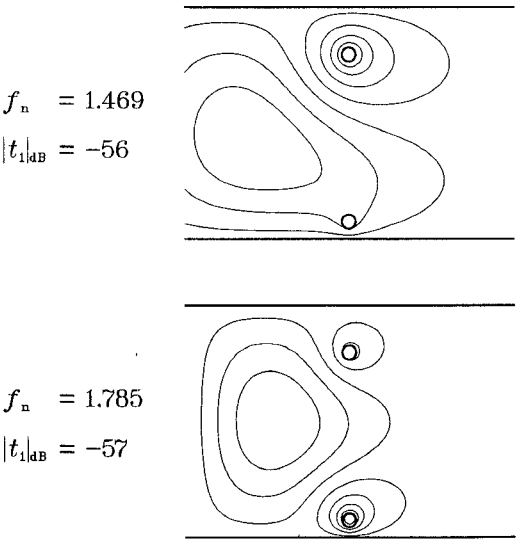

Fig. 7. Magnetic field in a bandstop filter with two dielectric posts at the two lowest resonance frequencies ($\omega t = 0.5\pi$):

$\epsilon_{r1} = 38.5$ $\epsilon_{r2} = 38.5$
$\tan\delta_1 = 2\times10^{-4}$ $\tan\delta_2 = 2\times10^{-4}$
$r_1 = 0.03h$ $r_2 = 0.03h$
$b_1 = 0.8h$ $b_2 = 0.075h$.

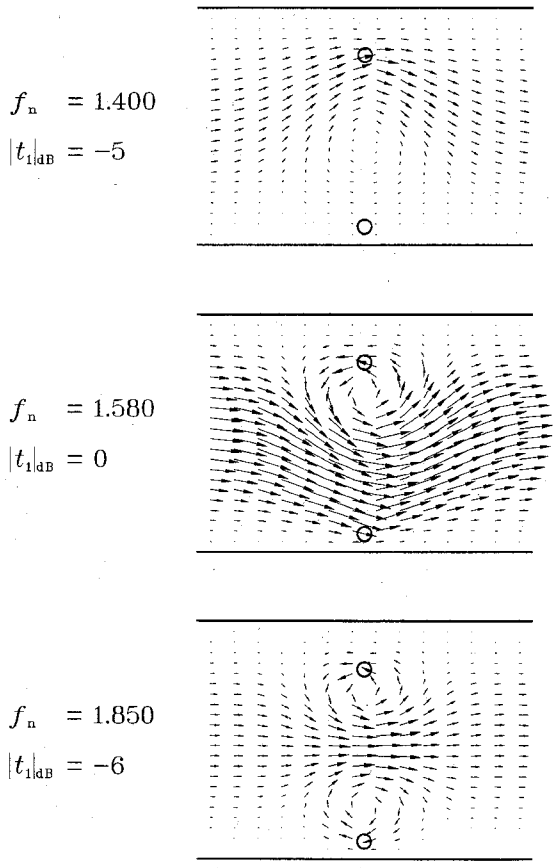

Fig. 8. Poynting vector in bandstop filter with two dielectric posts below, between, and above the two lowest resonance frequencies:

$\epsilon_{r1} = 38.5$ $\quad \epsilon_{r2} = 38.5$
$\tan\delta_1 = 2\times10^{-4}$ $\quad \tan\delta_2 = 2\times10^{-4}$
$r_1 = 0.03h$ $\quad r_2 = 0.03h$
$b_1 = 0.8h$ $\quad b_2 = 0.075h.$

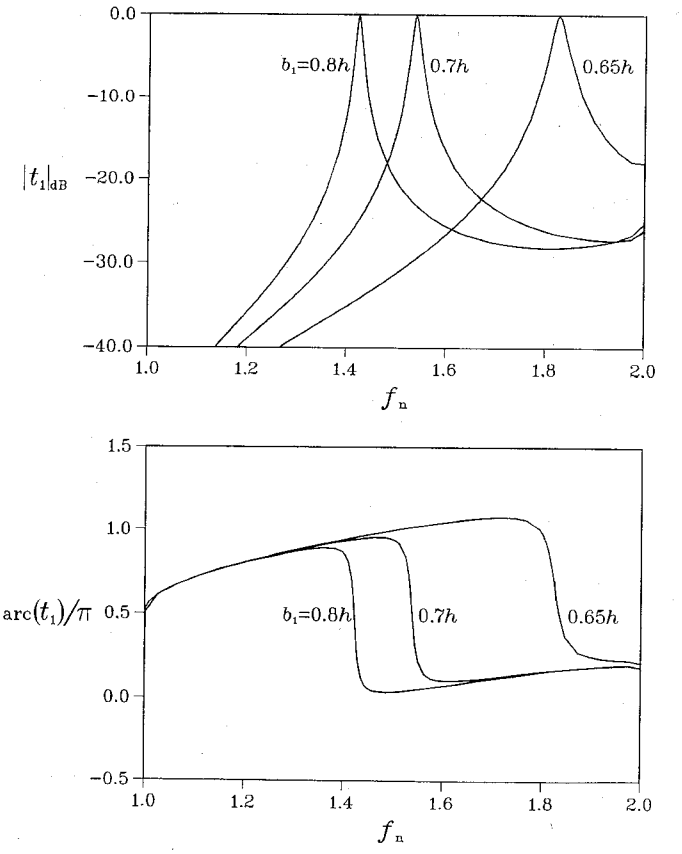

Fig. 9. Frequency responses of a tunable bandpass filter with one dielectric and one metallic post:

$\epsilon_{r1} = 38.5$ $\quad \epsilon_2 = -j\infty$
$\tan\delta_1 = 2\times10^{-4}$
$r_1 = 0.03h$ $\quad r_2 = 0.3h$
$b_1 = 0.65h \cdots 0.8h$ $\quad b_2 = 0.3h$
$R_1 = 0.2h$ $\quad R_2 = 0.3h.$

In all frequency responses, the normalized frequency f_n is used:

$$f_n = \frac{h}{2}\omega\sqrt{\epsilon_0\mu_0} = \frac{h}{\pi}k = \frac{f}{f_{c\,\mathrm{TE}_{10}}} \tag{18}$$

where $f_{c\,\mathrm{TE}_{10}}$ is the cutoff frequency of the fundamental TE_{10} mode. Together with the waveguide width h, used as a normalization length, the results can be applied to all waveguide bands used in practice.

A. Bandstop Filter

For all results given in this chapter, the sizes of the interaction regions are equal ($R_1 = R_2 = 0.25h$). A ceramic post material is chosen with high permittivity ($\epsilon_{ri} = 38.5$) and low loss ($\tan\delta_i = 2\times10^{-4}$). Although the post sizes are small ($r_1 = r_2 = 0.03h$), the lowest resonances occur in the fundamental frequency range of the rectangular waveguide ($1 \leqslant f_n \leqslant 2$).

The frequency responses for several post locations are shown in Figs. 4–6. They show t_1, the transmission coefficient of the fundamental TE_{10} mode defined by (8). If the geometry is symmetric, only one resonance occurs in the frequency range shown (Fig. 4, $b_2 = 0.2h$). Moving the lower post to the sidewall of the waveguide (Fig. 4, $0.2h \geqslant b_2 \geqslant 0.15h$), a second resonance occurs at a frequency different from the first resonance frequency. Further movement of the lower post (Fig. 5, $0.1h \geqslant b_2 \geqslant 0.05h$) increases the upper resonance frequency while the lower resonance frequency remains nearly constant. If the upper post is moved (Fig. 6), the lower resonance frequency can be tuned independently of the upper resonance frequency. This structure can be used as a tunable filter element with two stopbands. Each stopband can be tuned nearly independently of the other by moving one post.

A physical explanation of this effect is given by patterns of the magnetic fields (Fig. 7) and the Poynting vectors (Fig. 8). The stationary resonance fields are concentrated around the upper post at the lower resonance and around the lower post at the upper resonance (Fig. 7). The influence of moving the post on the frequency is related to the field energy concentration near the obstacle.

Now the field distributions in the cross sections of the waveguide will be discussed. At the lower resonance frequency, the fields beneath the posts are similar to the fields of the TE_{20} mode of the rectangular waveguide. At the upper resonance frequency, they are similar to the TE_{30} mode. The resonances can therefore be explained by

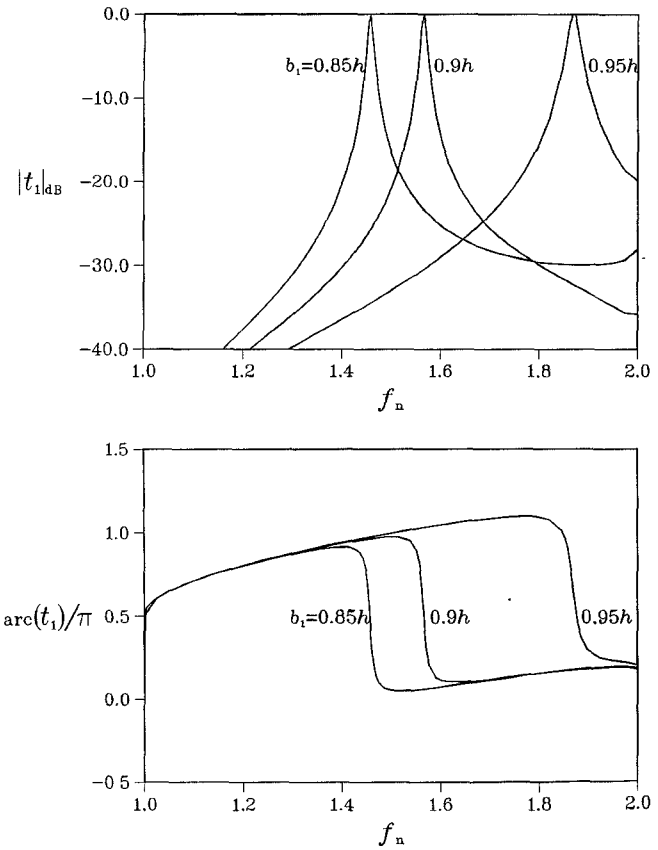

Fig. 10. Frequency responses of a tunable bandpass filter with one dielectric and one metallic post:

$\epsilon_{r1} = 38.5$	$\epsilon_2 = -j\infty$
$\tan\delta_1 = 2\times10^{-4}$	
$r_1 = 0.03h$	$r_2 = 0.3h$
$b_1 = 0.85h \cdots 0.95h$	$b_2 = 0.3h$
$R_1 = 0.2h$	$R_2 = 0.3h$.

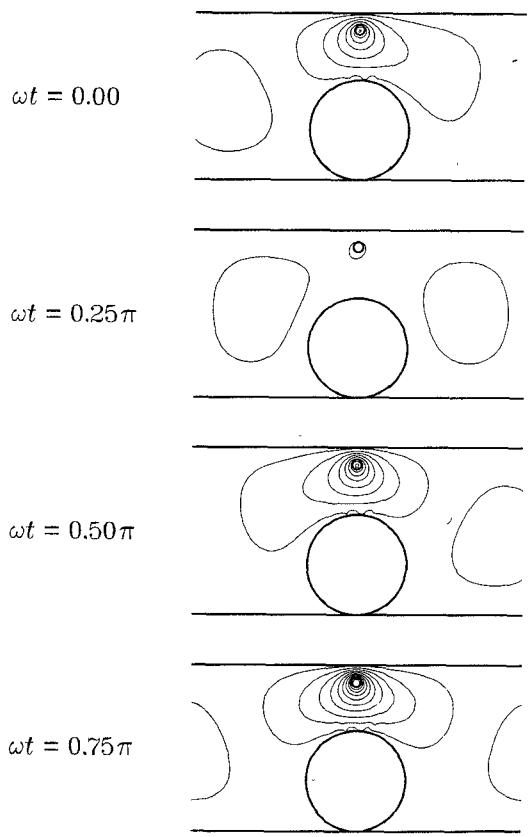

Fig. 11. Magnetic field in a bandpass filter with one dielectric and one metallic post at the lowest resonance frequency:

$f_n = 1.565$	$\lvert t_1\rvert_{dB} = -0.14$
$\epsilon_{r1} = 38.5$	$\epsilon_2 = -j\infty$
$\tan\delta_1 = 2\times10^{-4}$	
$r_1 = 0.03h$	$r_2 = 0.3h$
$b_1 = 0.9h$	$b_2 = 0.3h$
$R_1 = 0.2h$	$R_2 = 0.3h$.

the occurrence of higher order waveguide modes in a dielectric-loaded waveguide region. The lowest resonance is attached to the TE_{20} mode, the next to the TE_{30} mode. If the structure becomes symmetric, the TE_{20} mode is not excited, but the resonance frequency remains constant, so the occurrence of the resonance shown in Fig. 4 can be explained.

Fig. 8 shows the Poynting vectors below, between, and above the resonance frequencies. Below the lower resonance frequency the power flow from waveguide region W1 to region W2 is directed by a vortex located beneath the post with the greater distance to the sidewall. At frequencies between the two resonances, the power flow is directed by the post located close to the sidewall. Above the second resonant frequency, the influence of the two posts decreases and the power is transported nearly symmetrically between the posts. At the resonant frequencies, the vortex corresponding to the post causing the resonance changes its sense of rotation. This classification is in accordance with the comments on Fig. 7. Each occurring resonance adds one vortex. This can be explained by the waveguide modes in the way that each resonance is linked with an occurring waveguide mode and a new power distribution of the resonance fields.

B. Bandpass Filter

Frequency responses of the transmission coefficient of a bandpass filter with one large metallic and one small dielectric post are shown in Figs. 9 and 10. One passband is visible; the resonance frequency depends on the post position.

Patterns of the magnetic fields at different times are shown in Fig. 11; the corresponding Poynting vector diagram is given by Fig. 12. The waveguide region containing the large metallic post can be considered as a waveguide below its cutoff frequency. Only in the vicinity of the resonance of the small dielectric post is power transported from waveguide region W1 to region W2.

IV. Conclusions

A method is presented which provides accurate scattering parameters and field patterns for two cylindrical obstacles positioned in one cross section of a rectangular waveguide.

The two lowest resonances of a bandstop filter element with two dielectric posts are discussed. Resonance frequencies can be tuned by moving the posts. Each resonance can

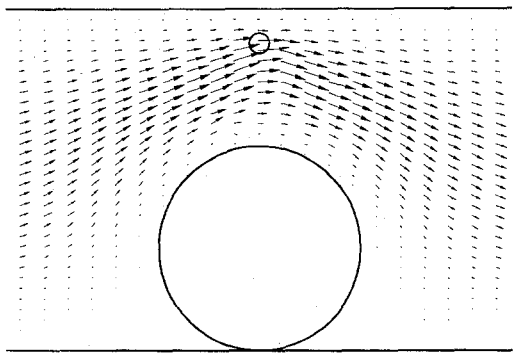

Fig. 12. Poynting vector in a bandpass filter with one dielectric and one metallic post at the lowest resonance frequency:

$$f_n = 1.565 \qquad |t_1|_{dB} = -0.14$$
$$\epsilon_{r1} = 38.5 \qquad \epsilon_2 = -j\infty$$
$$\tan\delta_1 = 2\times10^{-4}$$
$$r_1 = 0.03h \qquad r_2 = 0.3h$$
$$b_1 = 0.9h \qquad b_2 = 0.3h$$
$$R_1 = 0.2h \qquad R_2 = 0.3h.$$

be referred to one post and one waveguide mode to interpret the physical mechanism and the behavior of the resonance.

A bandpass filter can be realized by one metallic and one dielectric post.

ACKNOWLEDGMENT

The authors gratefully acknowledge the support given by Prof. Dr.-Ing. G. Piefke.

REFERENCES

[1] R. Gesche and N. Löchel, "Scattering by a lossy dielectric cylinder in a rectangular waveguide," *IEEE Trans. Microwave Theory Tech.*, vol. 36, pp. 137–144, Jan. 1988.

[2] R. Gesche, "Kreiszylindrische Streukörper im Rechteckhohlleiter," Darmstädter Dissertation D17, Darmstadt, West Germany, 1986.

[3] J. Lauterjung, "Abstrahlungs- und Beugungsprobleme in Hohlleiterstrukturen mit isotropen und magnetisch gyrotropen kreiszylindrischen Streukörpern," Darmstädter Dissertation D17, Darmstadt, West Germany, 1982.

[4] J. N. Sahalos and E. Vafiadis, "On the narrow-band microwave filter design using a dielectric rod," *IEEE Trans. Microwave Theory Tech.*, vol. MTT-33, pp. 1165–1171, 1985.

[5] P. G. Li, A. T. Adams, Y. Leviatan, and J. Perini, "Multiple-post inductive obstacles in rectangular waveguide," *IEEE Trans. Microwave Theory Tech.*, vol. MTT-32, pp. 365–373, 1984.

[6] G. S. Shaeffer and Y. Leviathan, "Composite inductive posts in waveguide—A multifilament analysis," *IEEE Trans. Microwave Theory Tech.*, vol. 36, pp. 779–783, 1988.

[7] C. G. Hsu and H. A. Auda, "Multiple dielectric posts in a rectangular waveguide," *IEEE Trans. Microwave Theory Tech.*, vol. MTT-34, pp. 883–891, 1986.

[8] C. G. Hsu and H. A. Auda, "On the realizability of the impedance matrix for lossy dielectric posts in a rectangular waveguide," *IEEE Trans. Microwave Theory Tech.*, vol. 36, pp. 763–765, 1988.

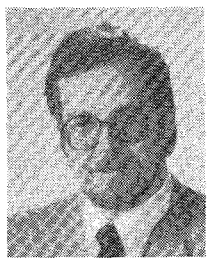

Roland Gesche (M'87) was born in Berlin, Germany, on June 18, 1957. He received the Diplom-Ingenieur and the Doktor-Ingenieur degrees from the Technical University of Darmstadt, Darmstadt, Germany, in 1982 and 1986, respectively.

From 1982 to 1987 he was employed as a research assistant at the Technical University of Darmstadt, where he was engaged in the theoretical investigation of microwave structures. Since 1987 he has been developing high-frequency and microwave equipment for physical vapor deposition and etching processes at Leybold AG, Alzenau, Germany.

Norbert Löchel was born in Marburg, Germany, on August 1, 1958. After receiving the Diplom-Ingenieur degree from the Technical University of Darmstadt, Darmstadt, Germany, he joined Siemens AG, München, where he is engaged in the development of microwave systems.